IMPACT OF INITIAL CONDITIONS ON THE EFFECTIVENESS OF ROLLING DYNAMIC COMPACTION OF GRANULAR SOILS

Andrew C. Bradley, Mark B. Jaksa, Yien-Lik Kuo
School of Architecture and Civil Engineering, University of Adelaide, Australia

https://doi.org/10.56295/AGJ5922

ABSTRACT

A finite element model (FEM) of rolling dynamic compaction (RDC) technology of a BH-1300 4-sided 8-tonne impact roller, developed previously by the authors, has shown to have reasonable agreement with that observed in the field. The use of this FEM is likely to provide high fidelity insights into the capability of the BH-1300 4-sided 8-tonne impact roller, namely in predicting the settlement and densification of an underlying granular material. A parametric study utilising this FEM with respect to initial density and shear strength parameters is undertaken to explore the relationship these properties have to the settlement and densification of a soil subject to RDC with a BH-1300 4-sided 8-tonne impact roller. The empirical relationships constructed within this study are validated against field trials from the literature of the roller improving sandy gravel fill at typical operating speeds of 10 km/h.

1 INTRODUCTION

Rolling dynamic compaction (RDC) technology involves the use of a heavy non-cylindrical rolling module incorporating 3, 4 or 5 sides to compact an underlying soil dynamically. In an effort to investigate the ground improvement effectiveness of RDC with a BH-1300 4-sided 8-tonne impact roller, Bradley et al. (2023) developed a transient non-linear finite element model (FEM), using LS-DYNA (LSTC, 2015), to reproduce, with good agreement, the settlement and densification of a coarse-grained soil for a given number of passes (N). The FEM had been developed to numerically simulate the motion and energy characteristics of the impact roller as reported by Bradley et al. (2019). Further, as presented by Bradley et al. (2024), the FEM has capability in investigating the ground response, producing estimates for the peak particle acceleration, peak particle velocity, and the peak in situ stresses.

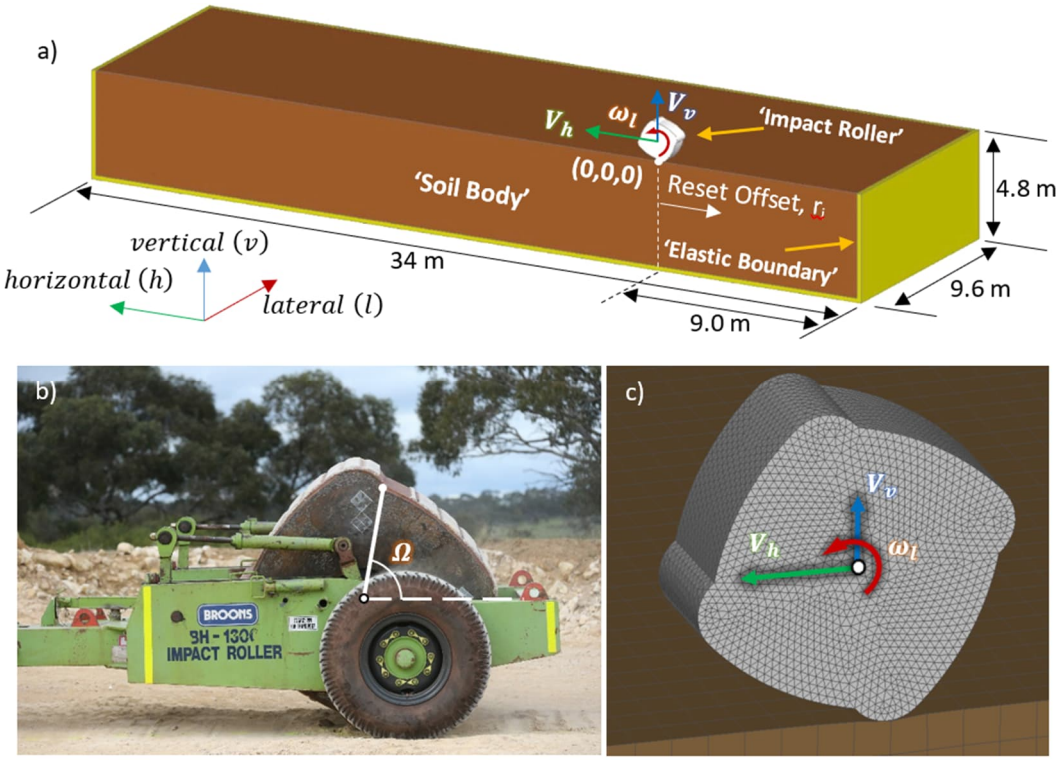

Figure 1: a) Global model layout in LS-DYNA; b) Broons BH 1300, 4-sided, 8-tonne impact roller prototype; and c) Broons BH 1300, 4-sided, 8-tonne impact roller FE mesh

The FEM utilises the geological cap model (GCM), supplied within LS-DYNA as Mat_025, to suitably represent volumetric behaviour, in addition to shear yield behaviour, of a soil. Prior approaches had typically utilised material models without adequately representing volumetric behaviour. As stated by Bradley et al. (2023), the material model is not without limitation. The GCM's formulation does not consider vibration-induced compaction. Despite this, it has been shown to reasonably reproduce observations in the field and thus is considered again in this study.

This paper aims to explore the effectiveness of RDC with a BH-1300 4-sided 8-tonne impact roller by undertaking a parametric study of the soil behaviour utilising the FEM and the methodology presented by Bradley et al. (2023), as summarised in Figure 1. First, the effective cohesion (c') of the soil body is explored, holding all else constant, to validate the assumption of using the apparent peak shear strength envelope of the soil by Bradley et al. (2023). Secondly, the effects of the initial void ratio (e_0) of the soil body, and thereby the initial relative density (Dr_0), Equation (1), on the effectiveness of the impact roller is explored, holding all else constant; where the maximum and minimum void ratio (e_{max} and e_{min}) reported by Bradley et al. (2023) are maintained at 0.816 and 0.328, respectively.

$$Dr_0 = \frac{e_{max} - e_0}{e_{max} - e_{min}} \tag{1}$$

2 METHODOLOGY

A finite element (FE) analysis is performed, using LS-DYNA, of a multiple pass scenario of the 4-sided 8-tonne impact roller undertaking $N = 30$ passes, 10 impacts per pass, using the FEM formulation and methodology presented by Bradley et al. (2023). The numerical efficacy of two FE mesh resolutions, namely $100\ mm \times 100\ mm \times 100\ mm$ and $200\ mm \times 200\ mm \times 200\ mm$ were examined by Bradley et al. (2023). Understandably, improved performance was observed with the finer mesh. Both the fine and coarse meshes are examined in the parametric investigation of c', however due to constraints associated with super-computing resources, only the coarser FE mesh is explored for Dr_0.

As explained by Bradley et al. (2023), at the beginning of each subsequent pass, the module is returned to the start of the lane, with respect to the position of the roller in Figure 1a. To distribute the disturbance of the surface soils upon lowering of the module during the resetting phase, and to simulate the somewhat random positioning of the roller that occurs in the field, a variable reset offset (r_i), is adopted in the FEM simulations. The set of r_i as used by Bradley et al. (2023) is also adopted in this study.

Additionally, a static and constant vertical loading (L) is added to each of the 22,216 nodes of the roller. As explained by Bradley et al. (2023), this loading represents the additional loading provided to the roller by the double-spring-linkage mechanism, where Clifford & Bowes (1995) stated it increases the roller fall speed by 10 to 20%. Further, this additional loading acts to account for error in the contact interaction between the roller and soil surface. To assist in providing resistance to erratic 'skipping motion', due to error in the roller-soil interaction due a change in initial conditions, $L = 1$ N is selected (Bradley et al., 2023).

2.1 SOIL PROPERTIES

Holding all else constant, the parametric study of the soil properties used by Bradley et al. (2023) is undertaken with respect to varying c' and then Dr_0.

To explore the dependence on the shear strength properties of the soil and the appropriateness of using the apparent peak effective cohesion of $c' = 13.5\ kPa$ in lieu of using kinematic hardening, a parametric investigation, with respect to c' of the soil body, is undertaken. Here, $c' = 50$ kPa is selected to be representative of an upper value of shear strength brought about by kinematic hardening and/or fine-grained content; and $c' = 1$ kPa is representative of a coarse-grained material that exhibits no increase in shear strength when subjected to an elevated strain rate. Between them, the approach of selecting the apparent peak effective cohesion of the soil is explored, as measured from a triaxial performed at an elevated strain rate, which seeks to represent the soil's behaviour during RDC.

Thereafter, a parametric study of e_0, and thereby Dr_0, of the soil body is undertaken to explore their impact on the outcome of the FEM. The volumetric behaviour is constructed with respect to the intercept of the virgin compression line (VCL) (e_L), logarithmic slope of the VCL (λ), and the logarithmic slope of the unload-reload line (URL) (κ), as reported by Bradley et al. (2023), and five selected values of e_0, as shown in Figure 2. The apparent preconsolidation pressure (p_c) intercept of the VCL and the initial URL for each given e_0, is calculated from Equation (2).

$$p_c = \exp\left[\frac{e_L - e_0}{\lambda - \kappa}\right] \tag{2}$$

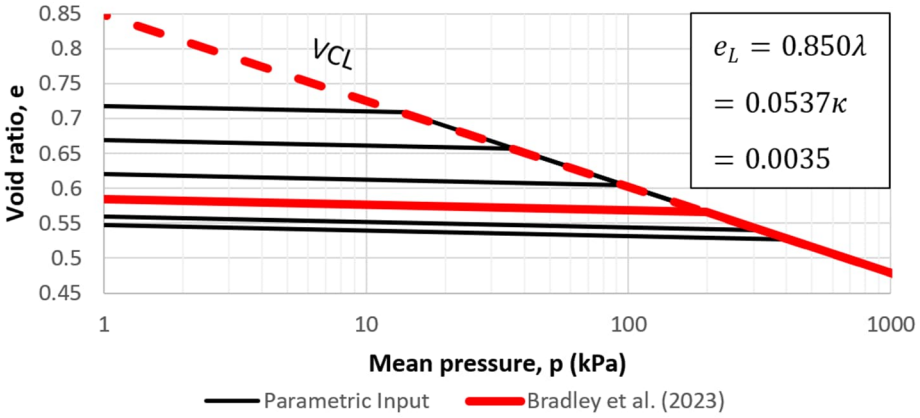

Figure 2: Spread of parametric study with respect to volumetric behaviour

The calculation of the GCM (i.e. Mat_025) input follows the methodology presented by Bradley et al. (2023). The maximum pressure (p_{max}) of 1.2 MPa, as used by Bradley et al. (2023, 2024), based upon field observations by Scott et al. (2019a, 2019b), is maintained for consistency. A summary of the parametric inputs is presented in Table 1.

Table 1: Summary of inputs for GCM (i.e. Mat_025)

Initial Conditions			Mass Density	Elasticity		Cohesion	Plastic Volumetric Strain	
c′	Dr_0 (e_0)	p_c	ρ	K	G	α	D	W
kPa	% (-)	kPa	t/mm^3	MPa	MPa	MPa	MPa^{-1}	-
1	47.7% (0.585)	197	1.880E-09	44.94	16.10	0.00342	0.5028	0.0572
13.5	47.7% (0.585)	197	1.880E-09	44.94	16.10	0.04618	0.5028	0.0572
50	47.7% (0.585)	197	1.880E-09	44.94	16.10	0.17104	0.5028	0.0572
13.5	20% (0.718)	14	1.733E-09	48.73	17.45	0.04618	1.2441	0.1303
13.5	30% (0.670)	37	1.784E-09	47.34	16.96	0.04618	0.9734	0.1050
13.5	40% (0.621)	97	1.838E-09	45.96	16.46	0.04618	0.7018	0.0780
13.5	52.5% (0.560)	321	1.909E-09	44.24	15.85	0.04618	0.3670	0.0424
13.5	55% (0.548)	417	1.924E-09	43.89	15.72	0.04618	0.2942	0.0343
Note: $\gamma = \beta = T = \bar{C} = \bar{N} = 0$; $X_0 = 0.003\ MPa$; $\theta = 0.302$; and $R = 3.3075$								

Where: ρ is the mass density; K is the elastic bulk modulus; G is the elastic shear modulus; $\alpha, \beta, \gamma, \theta, R, T$ are shear envelope parameters; D, W, X_0 are plastic volumetric strain parameters; and $\bar{C}, \bar{N}$ are kinematic hardening parameters (LSTC, 2015).

3 NUMERICAL MODELLING

This section presents the results of the numerical modelling, which was undertaken using the University of Adelaide's super-computing facility, Phoenix, which incorporates 2 × Intel Xeon Gold 6248 Processors @ 2.4 GHz and 12 CPU cores. Firstly, a parametric study with respect to c' is discussed in §3.1, and the parametric analyses with respect to Dr_0 are subsequently presented in §3.2.

3.1 RESULTS – COHESION

A multiple pass scenario for $N = 30$ passes of the BH-1300, 4-sided 8-tonne impact roller was undertaken with respect to $c' = 1, 13.5, \text{and } 50$ kPa with both the fine and coarse FE meshes. As will be discussed further below, the results show that the FEM is sensitive to small values of c', chiefly for $c' = 1$ kPa, whereby the dilation from shearing is overly significant.

3.1.1 Roller motion and energy delivered

The resulting vertical velocity (V_v, Fig. 1c), kinetic energy and total energy time histories of the roller with respect to the roller's orientation (Ω, Fig. 1b) are benchmarked against the typical motion described by Bradley et al. (2019). For the most part, the FEMs reproduced a conforming representation of the kinematic profile of the BH-1300, 4-sided 8-tonne impact roller. This is despite prescribing a single set of r_i and is likely due to the assistance of selecting the additional loading of $L = 1$ N per node of the roller. As per Table 2, the roller's peak kinetic energy $\left(E_{kinetic}^{peak}\right)$ and total energy lost (E_{lost}) through each impact, and the magnitude of energy absorbed by the soil per impact $(E_{absorbed})$ among the FEMs is in good agreement with the field validated observations of Bradley et al. (2019). Likely due to discretization error, the coarser FE mesh yields a greater sensitivity with respect to c'. Nevertheless, the results for both FE meshes conform with that observed by Bradley et al. (2019).

Table 2: Summary of resulting energy parameters from c' parametric study

FE Mesh Resolution	c' (kPa)	$E_{kinetic}^{peak}$ (kJ)*	E_{lost} (kJ)*	$E_{absorbed}$ (kJ)*	Conforms with Bradley et al. (2019)
200 x 200 x 200 mm	1	63.6 ± 0.2	23.4 ± 0.7	20.7 ± 1.1	Yes
	13.5	63.3 ± 0.2	21.0 ± 0.6	19.4 ± 0.8	Yes
	50	63.3 ± 0.2	21.5 ± 0.5	18.6 ± 1.0	Yes
100 x 100 x 100 mm	1	63.0 ± 0.3	22.9 ± 0.7	20.4 ± 1.5	Yes
	13.5	63.5 ± 0.2	21.6 ± 0.6	20.6 ± 1.4	Yes
	50	63.9 ± 0.2	21.3 ± 0.5	20.5 ± 1.1	Yes
Note: *: at 95% confidence					

3.1.2 Surface settlement

The range of settlement with respect to each pass, along the length of interest subject to $N = 30$ passes and horizontal chainages from 3.4 m to 8.8 m, is benchmarked against Scott et al. (2016), as summarised in Figure 3. As can be seen in Figure 3a, the FEM with $c' = 1$ kPa predicts the surface to heave significantly as a result of the dilation due to shearing, whereas the predicted settlements are reasonably consistent with the field observations for $c' = 13.5$ and 50 kPa.

The magnitude and depth of heaving is unlikely to be representative and highlights the need for the soil body to be defined with sufficient c'. Evidently, the dynamic nature of the loading invokes and requires an added strength to the soil within the FEM. Further, although some dilation is expected, it would appear that the model may overrepresent the magnitude of dilation as surface elements continued to expand seemingly without limit for $c' = 1$ kPa. Lastly, the FE mesh resolution has little bearing on the settlement estimates.

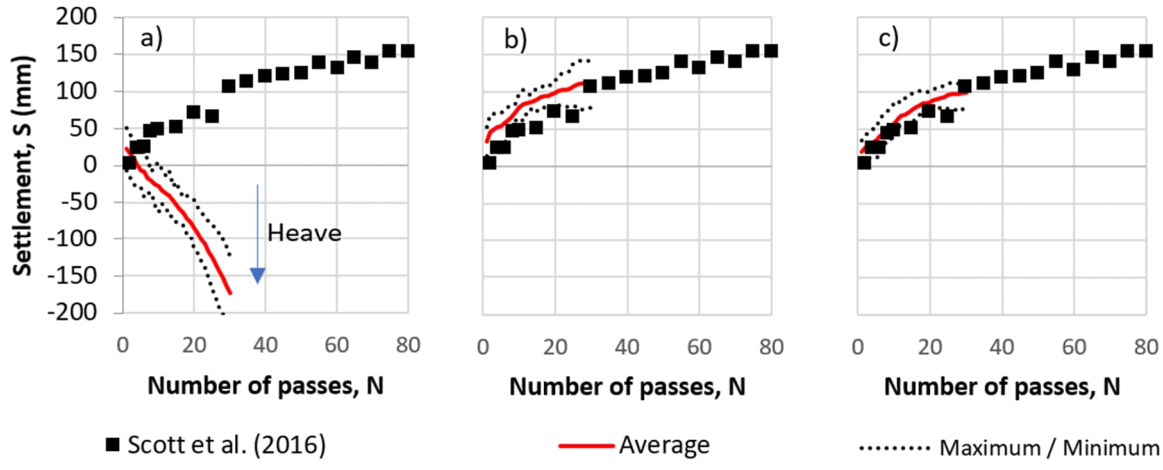

Figure 3: Surface settlement: c' = a) 1 kPa; b) 13.5 kPa; and c) 50 kPa [$100\ mm \times 100\ mm \times 100\ mm$ FEs]

3.1.3 Compaction

Consistent with the methodology of Bradley et al. (2023), at the conclusion of each pass, the magnitude of compaction is estimated along the length of interest, underneath the width of the roller, and assessed in terms of the improvement index, I_r, which is calculated by Equation (3), as shown in Figure 4. The I_r vs depth (d) curves for $N = 5, 10$ and 30 passes are plotted alongside the I_r values inferred from the dynamic cone penetration (DCP) test (Standards Australia, 1997) and nuclear densometer test (Standards Australia, 2007) field results, as presented by Bradley et al. (2023).

In summary, low shear strength, i.e. $c' = 1$ kPa, exhibits dilation due to shearing which extends below the ground surface and infers a very limited ability to improve the soil. Whereas there is reasonable consistency between $c' = 13.5$ and 50 kPa, although increasing improvement with increasing c'. The significant outcome of the study is that the use of the apparent peak shear strength, $c' = 13.5$ kPa, in lieu of kinematic hardening, is a sufficient approach.

$$I_r = \frac{Dr - Dr_0}{1 - Dr_0} \tag{3}$$

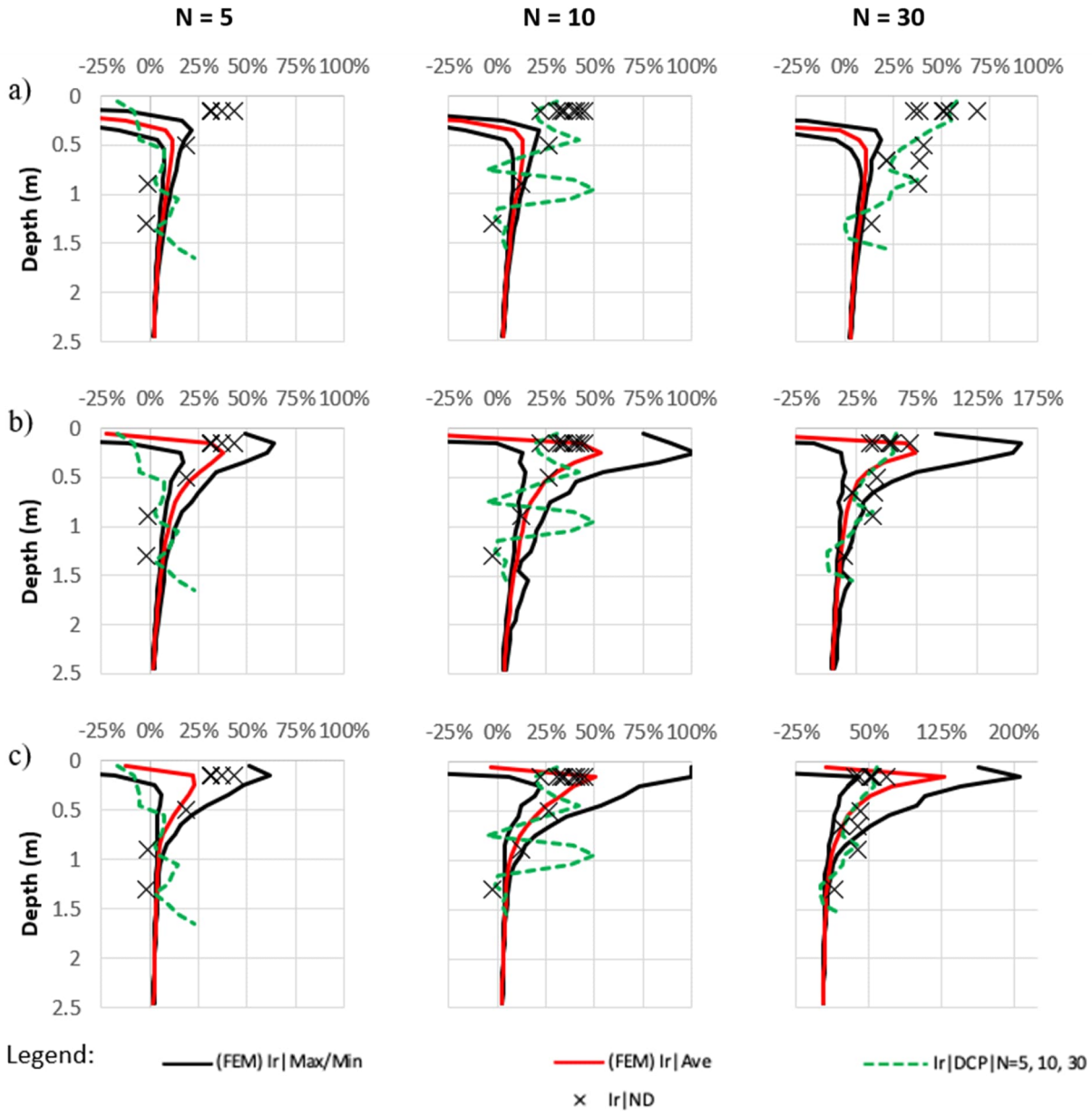

Figure 4: Improvement index profiles for N = 5, 10 and 30 passes [using $100\ mm \times 100\ mm \times 100\ mm$ FEs]: a) c' = 1 kPa; b) c' = 13.5 kPa; and c) c' = 50 kPa

3.2 RESULTS – INITIAL DENSITY

A multiple pass scenario for $N = 30$ passes of the BH-1300, 4-sided 8-tonne impact roller was undertaken with respect to $Dr_0 = 30, 40, 52.5$ and 55%. The FEM for $Dr_0 = 20\%$ failed as a result of numerical errors after $N = 17$ passes due to significantly large strains, despite LS-DYNA's ability to manage large deformations. The results show that the FEM is sensitive to the input Dr_0. As expected, significant large strain deformations are experienced for looser material, and lessens with denser materials. The effectiveness of RDC appears to become limited in the presence of initially denser material such that in modelling RDC using the FEM by Bradley et al. (2023) it may only be applicable for soils where $30 \leq Dr_0 \leq 55\%$ or $p_c \leq 417$ kPa, as defined in Equations (1) and (2), respectively. Note that $Dr_0 = 100\%$, is indicative of where $e_0 = e_{\min}$. Bradley et al. (2023) selected their $e_{\min}$, which is consistent with that adopted in the present study, as that associated with the maximum dry density of the soil as measured by the modified Proctor test (Standards Australia, 2017).

3.2.1 Roller motion and energy delivered

As summarised in Table 3, and similar to that reported previously in §3.1.1, the average energy delivered by the fine and coarse FE models is consistent with that measured in the field by Bradley et al. (2019), despite the difference in initial conditions. Notably, although expected, there is a significant trend of diminution of $E_{absorbed}$ against increasing Dr_0, as less soil is compacted.

Table 3: Summary of resulting energy parameters from Dr_0 parametric study

Mesh Resolution	Dr_0 (%)	$E_{kinetic}^{peak}$ (kJ)*	E_{lost} (kJ)*	$E_{absorbed}$ (kJ)*	Conforms with Bradley et al. (2019)
200 x 200 x 200 mm	20	62.6 ± 0.4	22.8 ± 1.1	23.7 ± 2.4	Yes
	30	62.9 ± 0.3	22.0 ± 0.7	21.2 ± 1.4	Yes**
	40	63.2 ± 0.2	21.3 ± 0.7	20.1 ± 1.2	Yes
	47.4	63.3 ± 0.2	21.0 ± 0.6	19.4 ± 0.8	Yes
	52.5	63.4 ± 0.2	21.0 ± 0.4	18.4 ± 0.8	Yes
	55	63.6 ± 0.2	21.1 ± 0.4	18.4 ± 1.0	Yes
Note: *: at 95% confidence; **: observed a 'skipping motion' for at least one impact					

3.2.2 Surface settlement

The range of settlement with respect to each pass along the length of interest is examined and the average settlement with respect to N and Dr_0 is presented in Figure 5. As expected, the looser, more readily compressible material, incurs a greater surface settlement. Trends for the range of settlement produced between the FEMs can be reasonably reproduced by Equations (4), (5) and (6); for $20\% \leq Dr_0 \leq 55\%$.

In practice, the number of passes of RDC is often based upon achieving effective refusal (Avalle & McKenzie, 2005), as the change in settlement approaches zero. The trends identified herein present a means of predicting the number of passes necessary to achieve *effective refusal*. Further, as expected, the trends suggest initially softer material will require a greater number of passes to reach *effective refusal*.

$$\hat{S}_{max}(N, Dr_0) = (104.2 - 15.412 \cdot \mathrm{e}^{3.548 \cdot Dr_0}) \cdot \ln(N) + 153.58 \cdot e^{-3.885 \cdot Dr_0} + 15.3 \quad (4)$$

$$\hat{S}_{ave}(N, Dr_0) = (114.0 - 22.967 \cdot \mathrm{e}^{2.932 \cdot Dr_0}) \cdot \ln(N) + 138.25 \cdot e^{-3.679 \cdot Dr_0} - 2.2 \quad (5)$$

$$\hat{S}_{min}(N, Dr_0) = (148.0 - 47.417 \cdot \mathrm{e}^{2.050 \cdot Dr_0}) \cdot \ln(N) + 95.23 \cdot e^{-3.370 \cdot Dr_0} - 17.0 \quad (6)$$

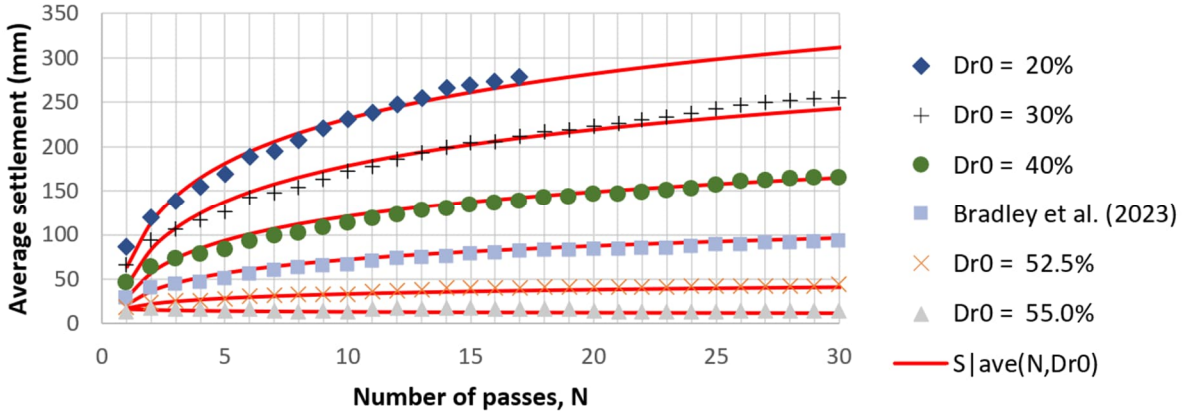

Figure 5: Summary of average settlement with respect to N and Dr_0

3.2.3 Compaction

As in §3.1.3, at the conclusion of each pass, the magnitude of compaction is estimated along the length of interest, beneath the width of the roller, and assessed in terms of I_r, as presented in Figure 6. As expected with more readily compressible material, with smaller values of Dr_0 and p_c, the magnitude of improvement at depth increases as a greater proportion is compressed. Further, there is an increasing amount of disturbance of near-surface soil with denser material, representative of over compaction as observed in the field by Clifford (1978).

The improvement indices with respect to Dr_0, d and N, directly beneath the impact roller along the lane and for the conditions modelled, may be reasonably reproduced by Equations (7), (8) and (9); for $N \geq 5$ passes, $20\% \leq Dr_0 \leq 55\%$. Using an average value of Dr_0 for each respective field trial, Figure 7, the proposed formulae are in good agreement with field measurements reported by Scott et al. (2016) and Bradley et al. (2023).

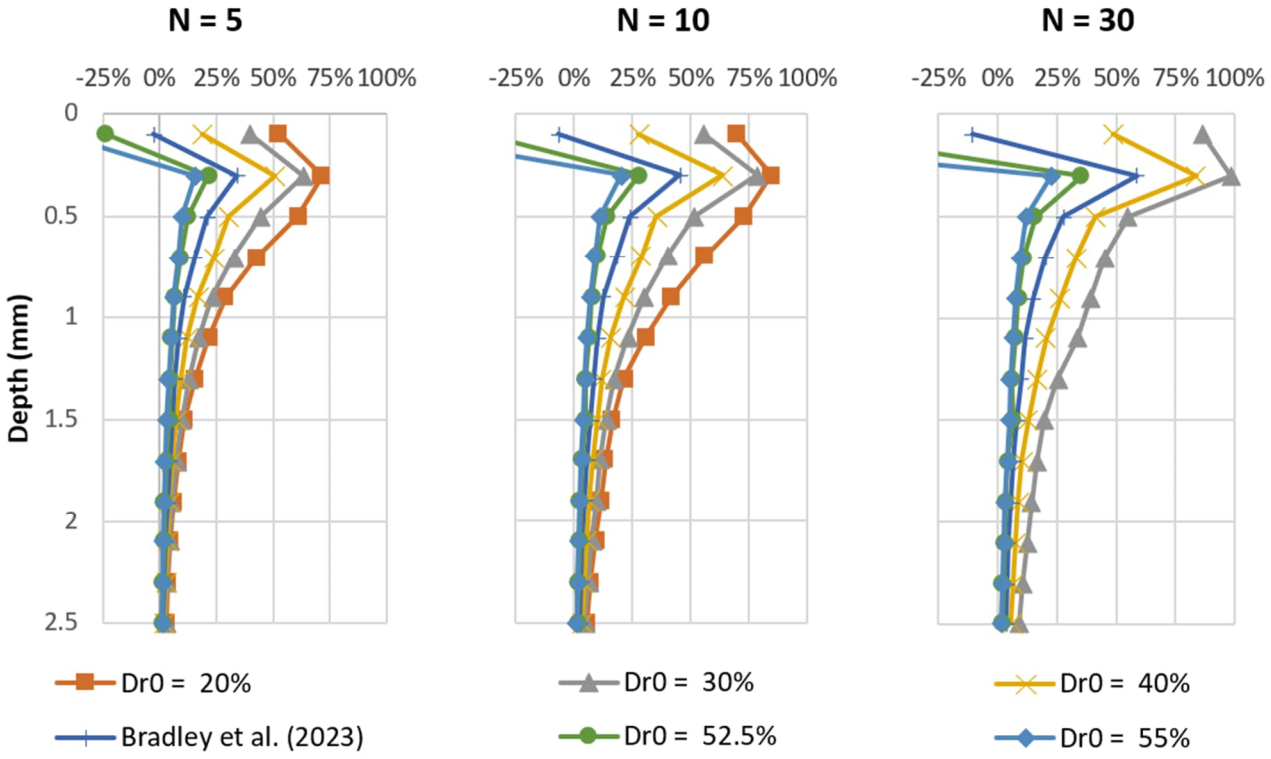

Figure 6: Distribution of average I_r with respect to Dr_0 and depth

$$\widehat{I}_{r_{max}}(N, Dr_0, d) = \begin{cases} [0.892 - (1.948 \cdot Dr_0^2 - 1.192 \cdot Dr_0 + 1.084)^{10}] \\ +[0.459 - (-7.916 \cdot Dr_0^2 + 6.045 \cdot Dr_0 - 0.884)^{0.474}] \\ [-5.736 \cdot Dr_0^2 + 3.291 \cdot Dr_0 + 0.025] \cdot \ln(N) \\ +[2.884 \cdot Dr_0^2 - 2.613 \cdot Dr_0 + 0.705] \\ \left[(0.238 - 0.415 \cdot Dr_0) \cdot d^{253.5 \cdot Dr_0^3 - 276.7 \cdot Dr_0^2 + 94.8 \cdot Dr_0 - 11.5}\right] \cdot \ln(N) \\ +\left[(25.2 \cdot Dr_0^3 - 32.26 \cdot Dr_0^2 + 12.05 \cdot Dr_0 - 0.82) \cdot e^{d \cdot (0.09 \cdot \ln(Dr_0) - 1.3)}\right] \\ -[68.69 \cdot Dr_0^4 - 114 \cdot Dr_0^3 + 68.29 \cdot Dr_0^2 - 17.22 \cdot Dr_0 + 1.49] \end{cases} \quad \begin{array}{l} \text{For:} \\ d = 0.1\ m \\ \\ d = 0.3\ m \\ \\ 2.5 \geq d \geq 0.5\ m \end{array} \tag{7}$$

$$\widehat{I}_{r_{ave}}(N, Dr_0, d) = \begin{cases} [0.407 - (1.694 \cdot Dr_0^2 - 0.879 \cdot Dr_0 + 0.960)^{10}] \cdot \ln(N) \\ +[0.502 - (-1.797 \cdot Dr_0^2 + 1.358 \cdot Dr_0 - 0.194)^{0.267}] \\ [0.226 - (0.0003 \cdot e^{11.512 \cdot Dr_0})] \cdot \ln(N) \\ +[0.728 - 0.2691 \cdot e^{1.672 \cdot Dr_0}] \\ \left[(0.145 - 0.257 \cdot Dr_0) \cdot d^{88.005 \cdot Dr_0^3 - 102.431 \cdot Dr_0^2 + 38.304 \cdot Dr_0 - 5.602}\right] \cdot \ln(N) \\ +\left[(1.357 - 2.251 \cdot Dr_0) \cdot e^{d \cdot (0.928 \cdot \ln(Dr_0) - 0.644)}\right] \\ +[15.528 \cdot Dr_0^4 - 26.639 \cdot Dr_0^3 + 16.570 \cdot Dr_0^2 - 4.379 \cdot Dr_0 + 0.398] \end{cases} \quad \begin{array}{l} \text{For:} \\ d = 0.1\ m \\ \\ d = 0.3\ m \\ \\ 2.5 \geq d \geq 0.5\ m \end{array} \tag{8}$$

$$\widehat{I}_{r_{min}}(N, Dr_0, d) = \begin{cases} [-0.008 - (-0.647 \cdot Dr_0^2 - 1.036 \cdot Dr_0 + 0.584)^{10}] \cdot \ln(N) \\ +[0.294 - (4.453 \cdot Dr_0^2 - 3.260 \cdot Dr_0 + 1.259)^{10}] \\ [-7.409 \cdot Dr_0^3 + 9.373 \cdot Dr_0^2 - 3.876 \cdot Dr_0 + 0.552] \cdot \ln(N) \\ -[2.680 \cdot Dr_0^2 - 1.211 \cdot Dr_0 - 0.131] \\ \left[(1.109 - 0.196 \cdot Dr_0) \cdot d^{1.786 \cdot Dr_0^3 - 2.478 \cdot Dr_0^2 + 1.195 \cdot Dr_0 - 0.209} - 1\right] \cdot \ln(N) \\ +\left[(36.5 \cdot Dr_0^3 - 41.8 \cdot Dr_0^2 + 13.3 \cdot Dr_0 - 0.7) \cdot e^{d \cdot (0.26 \cdot \exp(3.78 \cdot Dr_0) - 2.54)}\right] \\ +[17.71 \cdot Dr_0^4 - 22.34 \cdot Dr_0^3 + 9.56 \cdot Dr_0^2 - 1.56 \cdot Dr_0 + 0.08] \end{cases} \quad \begin{array}{l} \text{For:} \\ d = 0.1\ m \\ \\ d = 0.3\ m \\ \\ 2.5 \geq d \geq 0.7\ m \end{array} \tag{9}$$

Although, the foregoing presentation of results has identified trends between Dr_0 and the outcome of the FEMs, it may be more accurate to consider the relationship as being dependent on the p_c of the soil. As one might expect, this is likely due to RDC being less effective for initially denser materials, of which exhibit a higher p_c.

Bradley et al. (2024) estimated the impact roller to apply an average peak mean pressure ($\bar{p}^A$) through each impact of up to 455 kPa, as shown in Figure 8. Noting that, as Dr_0 approaches 55%, the p_c of the soil modelled in this study approaches 417 kPa. This explains why the roller becomes more limited in its ability to compact the soil beyond elastic volumetric strains, whilst accruing shear strains; or over compaction. The aforementioned trends can be converted with respect to p_c by Equation (10); where, $p_c \leq 417\ kPa$. However, a more sophisticated relationship between $e_0, e_L, e_{max}, e_{min}, \kappa, \lambda, p_c$ and the FEM output would require a more robust and exhaustive parametric study, which is beyond the scope of this study. Nevertheless, for soils of similar properties, the aforementioned formulae may prove beneficial for practicing engineers.

$$Dr_0 = \frac{e_{max} - e_L + (\lambda - \kappa) \cdot \ln(p_c)}{e_{max} - e_{min}} \tag{10}$$

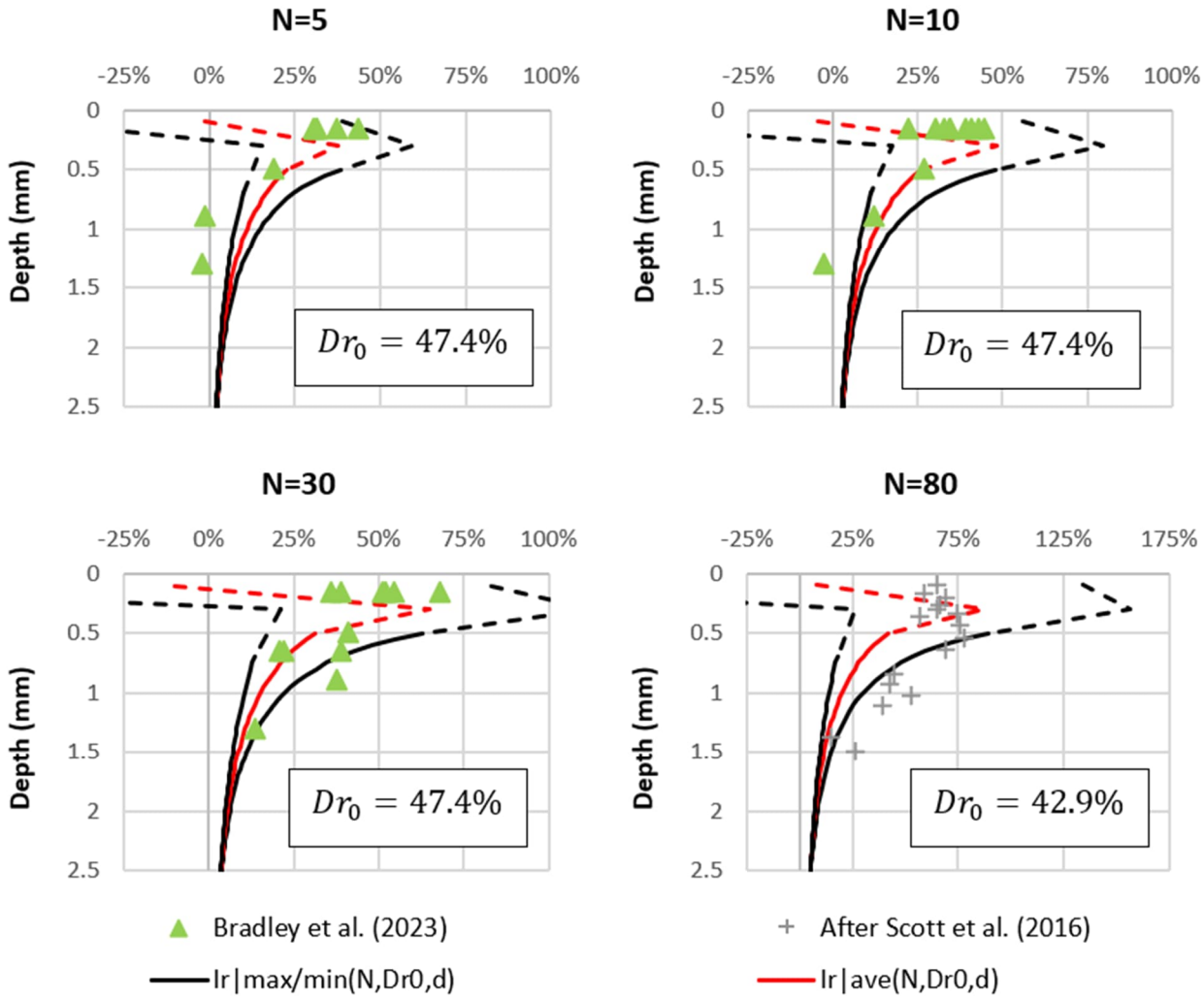

Figure 7: Range of I_r using proposed empirical expressions against field measurements

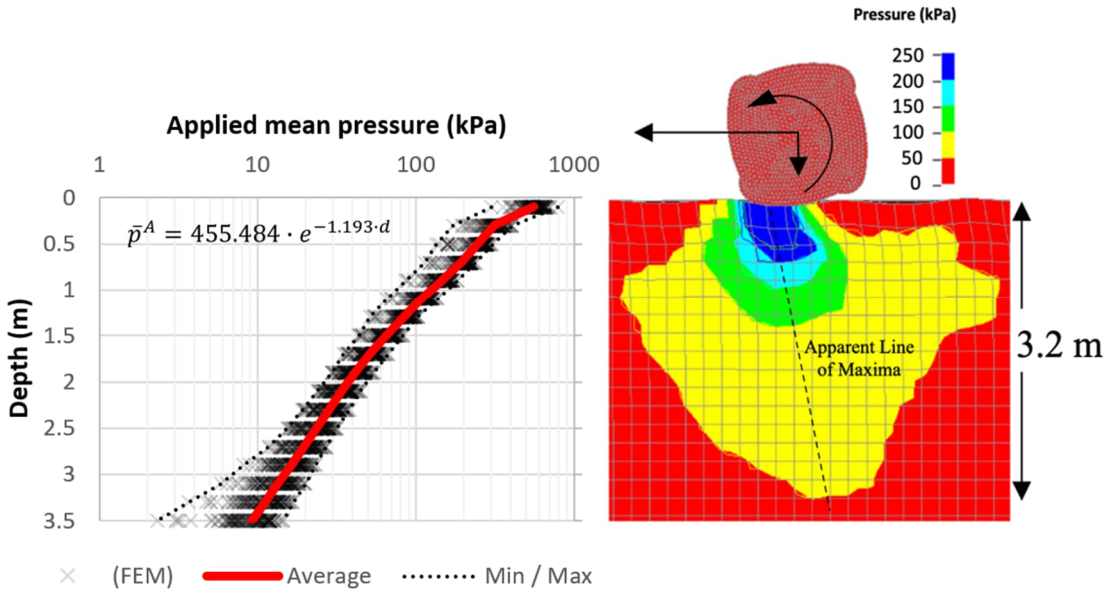

Figure 8: Peak in situ applied mean pressure ($\bar{p}^A$) (Bradley et al, 2024)

4 CONCLUSIONS

This paper presented results of a parametric study using a finite element (FE) simulation of rolling dynamic compaction (RDC) performed by a Broons BH-1300 4-sided 8-tonne impact roller on coarse-grained soil subjected up to 30 passes, using the formulation as presented by Bradley et al. (2023). The parametric study was undertaken with respect to the initial conditions of the granular materials, with respect to varying c' and then Dr_0; holding all else constant.

The results of the parametric study with respect to the cohesion of the material support the consideration by Bradley et al. (2023) in the use of the apparent peak effective cohesion $c' = 13.5$ kPa, as informed from their triaxial tests undertaken at elevated strain-rates. The FE analyses were shown to be sensitive to small values of c', chiefly for $c' = 1$ kPa, whereby the dilation from shearing is overly significant.

The results of the parametric study with respect to the initial density of the material provide insight into the relationship between Dr_0, or potentially p_c, and the resulting settlement and densification of the material. Of particular interest is the effectiveness of RDC and how it becomes more limited as Dr_0 trends towards 55%. Using the finite element model (FEM) formulation of Bradley et al. (2023), Bradley et al. (2024) estimated the impact roller to apply an average peak mean pressure through each impact of up to 455 kPa. Noting that, as Dr_0 approaches 55%, the p_c of the soil modelled in this study approaches 417 kPa. This likely explains why the effectiveness of the roller becomes more limited within the model, in its ability to compact the soil beyond elastic volumetric strains, whilst accruing shear strains, or over-compaction, which is a potential limitation of the formulation.

Further, as vibration-induced compaction has not been accounted for in the model, this presentation of results reflects the effectiveness borne from the kinematic compression of the soil delivered through RDC. However, if we were to account for vibration-induced compaction in addition to that borne from compression, the effectiveness of RDC would be higher for looser materials and may yet improve denser materials that would otherwise have limited improvement by compression alone.

Nonetheless, resulting from the parametric study, empirical formulae for estimating the range of settlement and improvement index at depth with respect to the number of passes and the initial density of the material were presented. From which, practicing engineers will have a greater understanding of the effectiveness of RDC with respect to differing initial conditions of granular materials, and estimating the minimum number of passes necessary to achieve effective refusal for them.

Using the proposed empirical formulae, the settlement and improvement index at depth may be estimated accounting for Dr_0 of the soil. However, these outcomes are reflective of the limitations of the FEM, and for soils akin to that modelled ($\lambda = 0.0537;\ \kappa = 0.0035;\ e_L = 0.850$). A more robust parametric study with respect to volumetric parameters λ, κ, e_L, in addition to e_0, may prove beneficial in constructing a generalised formula to predict the settlement and densification of granular soils. Thus, future studies would be served well by a robust investigation utilising the FE simulation approach with respect to varying soil conditions; ideally with a field or scale-model investigation.

Moreover, the resulting empirical formulae presented herein are reflective of the use of a coarser $200\ mm \times 200\ mm \times 200\ mm$ FE mesh resolution. Whereas, as stated by Bradley et al. (2023, 2024), improved results may be obtained with a finer FE mesh resolution, but the greater computational and post-processing cost is a significant limiting factor.

As stated by Bradley et al. (2024) and reiterated here, there is room to improve upon the model formulation of Bradley et al. (2023). One notable limitation is the absence of accounting for vibration-induced compaction effects within the GCM used in the FE simulation. Vibration-induced compaction, resulting from cyclic shearing forces generated by the impact roller, can influence the densification and settlement behaviour of the soil. However, the GCM utilized in this study does not explicitly incorporate these effects into the modelling framework. As a result, the simulation may not fully capture the complete range of ground improvement mechanisms associated with RDC, particularly in scenarios where vibration-induced compaction plays a significant role, such as for loose cohesionless materials.

Additional improvements to the formulation also include the consideration of multiple distinct layers, in place of a homogenous soil mass, each with their own geotechnical characteristics and behaviour, as is typically the case in the field. Another may be to consider a refined FE mesh resolution in the upper $1.5\ m$ of near surface soil to reduce the discretization error and achieve larger values of mean pressure as observed from field investigations.

5 ACKNOWLEDGEMENTS

The authors appreciate the assistance of Dr Brendan Scott and Mr Mark Innes at the University of Adelaide. The authors present their gratitude to the support team for the Phoenix High Performance Computing services at the University of Adelaide.

CRediT authorship contribution statement

Andrew C. Bradley: Conceptualization, Data curation, Formal Analysis, Investigation, Methodology, Software, Validation, Writing – original draft. **Mark B. Jaksa:** Supervision, Writing – review & editing. **Yien-Lik Kuo:** Supervision, Writing – review & editing.

6 REFERENCES

Avalle, D. L., & McKenzie, R. W. (2005). Ground improvement of Landfill site using the "square" impact roller. *Australian Geomechanics, 40*(4), 15-21.

Bradley, A. C., Jaksa, M. B., & Kuo, Y. L. (2019). Examining the kinematics and energy of the four-sided impact roller. *Proceedings of the Institution of Civil Engineers - Ground Improvement, 172*(4), 297-304.

Bradley, A. C., Jaksa, M. B., & Kuo, Y. L. (2023). Finite Element Modelling of Rolling Dynamic Compaction. *Computers and Geotechnics, 157*(105275). doi:10.1016/j.compgeo.2023.105275

Bradley, A. C., Jaksa, M. B., & Kuo, Y. L. (2024). Ground Response of Rolling Dynamic Compaction - a Finite Element Modelling Approach. *Frontiers in Built Environment*.

Clifford, J. M. (1978). *Evaluation of compaction plant and methods for the construction of earthworks in southern africa.* Durban, South Africa: MSE thesis, University of Natal.

Clifford, J. M., & Bowes, G. (1995). *Calculating the energy delivered by an impact roller. A trilogy of Papers for the Sept. 1995 Lecture Tour and International Seminars to commemorate the 10th Anniversary of the BH 1300 Standard Impact Roller, Paper Two.*

LSTC. (2015). *LS-DYNA Keyword User's Manual.* Livermore, California: Livermore Software Technology Corporation.

Scott, B. T., Jaksa, M. B., & Mitchell, P. (2019a). Ground response to rolling dynamic compaction. *Géotechnique Letters, 9*(2), 99-105.

Scott, B. T., Jaksa, M. B., & Mitchell, P. (2019b). Depth of influence of rolling dynamic compaction. *Proceedings of the Institution of Civil Engineers - Ground Improvement*.

Scott, B. T., Jaksa, M. B., & Syamsuddin, E. (2016). Verification of an impact rolling compaction trial using various in situ testing methods. *Proceedings 5th International Conference on Geotechnical and Geophysical Site Characterisation*, (pp. 735-740). Gold Coast, Australia.

Standards Australia. (1997). *AS 1289.6.3.2: Methods of testing soils for engineering purposes Soil strength and consolidation tests - Determination of the penetration resistance of a soil - 9 kg dynamic cone penetrometer test.* Standards Australia.

Standards Australia. (2007). *AS 1289.5.8.1: Methods of testing soils for engineering purposes Soil compaction and density tests - Determination of field density and field moisture content of a soil using a nuclear surface moisture-Density gauge - Direct transmission mode.* Standards Australia.

Standards Australia. (2017). *AS 1289.5.2.1: Methods of testing soils for engineering purposes Soil compaction and density tests - Determination of the dry density/moisture content relation of a soil using modified compactive effort.* Standards Australia.